BIOCHEMISTRY
including biophysical chemistry & molecular biology

Article

pubs.acs.org/biochemistry

Crystal Structures of *Acetobacter aceti* Succinyl-Coenzyme A (CoA):Acetate CoA-Transferase Reveal Specificity Determinants and Illustrate the Mechanism Used by Class I CoA-Transferases

Elwood A. Mullins[†,‡] and T. Joseph Kappock*[,†]

[†]Department of Biochemistry, Purdue University, West Lafayette, Indiana 47907-2063, United States

[‡]Department of Chemistry, Washington University, St. Louis, Missouri 63130-4899, United States

Supporting Information

ABSTRACT: Coenzyme A (CoA)-transferases catalyze transthioesterification reactions involving acyl-CoA substrates, using an active-site carboxylate to form covalent acyl anhydride and CoA thioester adducts. Mechanistic studies of class I CoA-transferases suggested that acyl-CoA binding energy is used to accelerate rate-limiting acyl transfers by compressing the substrate thioester tightly against the catalytic glutamate [White, H., and Jencks, W. P. (1976) *J. Biol. Chem. 251*, 1688−1699]. The class I CoA-transferase succinyl-CoA:acetate CoA-transferase is an acetic acid resistance factor (AarC) with a role in a variant citric acid cycle in *Acetobacter aceti*. In an effort to identify residues involved in substrate recognition, X-ray crystal structures of a C-terminally His_6-tagged form (AarCH6) were determined for several wild-type and mutant complexes, including freeze-trapped acetylglutamyl anhydride and glutamyl-CoA thioester adducts. The latter shows the acetate product bound to an auxiliary site that is required for efficient carboxylate substrate recognition. A mutant in which the catalytic glutamate was changed to an alanine crystallized in a closed complex containing dethiaacetyl-CoA, which adopts an unusual curled conformation. A model of the acetyl-CoA Michaelis complex demonstrates the compression anticipated four decades ago by Jencks and reveals that the nucleophilic glutamate is held at a near-ideal angle for attack as the thioester oxygen is forced into an oxyanion hole composed of Gly388 NH and CoA N2″. CoA is nearly immobile along its entire length during all stages of the enzyme reaction. Spatial and sequence conservation of key residues indicates that this mechanism is general among class I CoA-transferases.

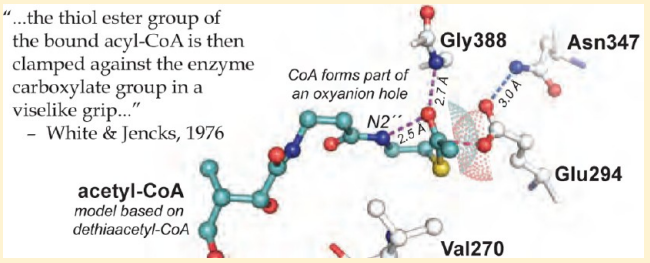

Coenzyme A (CoA)-transferases (EC 2.8.3) perform acyl transfer reactions involved in the metabolic activation of carboxylate substrates.[1] Class I CoA-transferases, typified by mitochondrial succinyl-CoA:3-oxoacid CoA-transferase (SCOT), form multiple covalent adducts involving an essential glutamate residue (Figure 1).[2−6] In the first half-reaction, the binary enzyme·acyl-CoA complex is converted into a CoA thiolate complex that also contains an acylglutamyl anhydride adduct. CoA thiolate then attacks the internal carbonyl to form a complex containing the carboxylate product and a glutamyl-CoA thioester. After carboxylate exchange, the second half-reaction proceeds by the opposite reaction sequence to form the acyl-CoA product complex. One or more of the binary complex interconversions illustrated in Figure 1 is rate-limiting in SCOT catalysis.[2] The acyl-CoA substrate binding energy is harnessed to accelerate catalysis in a process that immobilizes the acyl moiety[7,8] and requires an intact covalent link to unreacting parts of the acyl-CoA substrate.[9−11] Crystal structures show constriction of the enzyme around CoA,[12,13] but these interactions are not sufficient to account for rate accelerations achieved by the enzyme·acyl-CoA substrate complex.[1] While glutamyl-CoA thioester adduct structures are available (PDB entries 2ahw, 2oas, and 3oxo),[14,15] structures of a class I CoA-transferase bound to acyl-CoAs, carboxylates, and

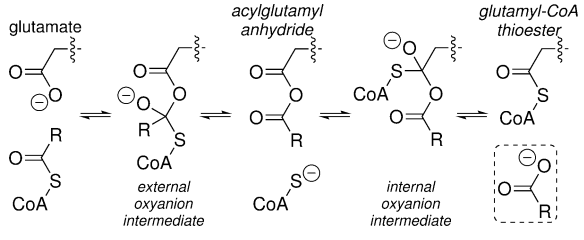

Figure 1. General half-reaction for class I CoA-transferases. Two tetrahedral oxyanion intermediates differ by whether CoA becomes attached to the external carbonyl, provided by the acyl-CoA/carboxylate substrate, or the internal carbonyl, provided by the essential active-site glutamate. Following exchange of the carboxylate product (dashed box), the second half-reaction proceeds in the reverse order of the first half-reaction.

Received: July 17, 2012
Revised: September 27, 2012
Published: October 2, 2012

 © 2012 American Chemical Society dx.doi.org/10.1021/bi300957f | *Biochemistry* 2012, 51, 8422−8434

anhydride adducts are still needed to explain how these enzymes transmute acyl-CoA binding energy into rate accelerations.[16]

Class I CoA-transferases have similar sequences, structures, and ping-pong kinetic mechanisms.[2] Class III CoA-transferases differ in all of these but use a chemically analogous reaction sequence involving anhydride and thioester adducts of an essential aspartate residue.[17] Crystal structures of adducts and complexes of *Oxalobacter formigenes* formyl-CoA transferase (FRC) have allowed the assembly of a structural model for the entire class III CoA-transferase reaction.[18,19] This reaction, however, relies upon substantial movement of the CoA pantetheine moiety. Conversely, evidence suggests that the reactive portion of the acyl-CoA substrate is tightly held in a single conformation throughout the class I reaction.[7,16] This difference may be indicative of two unique and class-specific catalytic mechanisms.

The class I CoA-transferase succinyl-CoA:acetate CoA-transferase (SCACT, AarC) is an acetic acid resistance factor that is required for acetate resistance[20,21] by vinegar factory strain *Acetobacter aceti* 1023.[22,23] Acetic acid bacteria (AAB) are acidophilic acetic acid producers that use diverse methods to cope with the constant influx of acetic acid from the culture medium.[24] Several AAB[25−27] use AarC in a variant citric acid cycle (CAC) that "overoxidizes" acetic acid to CO_2, which then diffuses into the acidic culture medium.[28] A privileged role in the *A. aceti* central metabolism and the link between CAC flux and the pivotal acetic acid resistance phenotype[24] would have imposed strong evolutionary selection for efficient catalysis by AarC.

Here we report the kinetic and structural characterization of AarC. These data were used to assemble a structural model for the AarC mechanism that is congruent with kinetic findings and can be applied to all class I CoA-transferases. Protein conformational changes assemble a chemically competent active site around a bound acyl-CoA substrate and regulate access to the catalytic pocket. In the closed conformation, the acyl-CoA thioester is pressed tightly against the active-site glutamate. Subsequent conversion to the glutamyl-CoA thioester and carboxylate product occurs with little motion of the enzyme or substrate. We propose that an auxiliary carboxylate binding site, located just outside the AarC catalytic pocket, contributes to the efficient recognition and conversion of the physiological carboxylate substrates.

EXPERIMENTAL PROCEDURES

Materials and Methods. Oligodeoxynucleotides [ODNs (Table S1 of the Supporting Information)] were obtained from IDT and used without further purification. DNA manipulations were performed using enzymes from New England Biolabs. DNA purification kits were from Qiagen. Plasmid pREP4-*groESL* was a gift from P. Cole.[29] Other reagents were from Sigma-Aldrich or Fisher Scientific. Dethiaacetyl-CoA was synthesized as described previously.[30] *A. aceti* citrate synthase with a C-terminal hexahistidine affinity tag was isolated as described previously.[30] Protein concentrations were measured using a Bio-Rad Bradford assay with crystalline bovine serum albumin as the standard.[31] Absorbance measurements were recorded on a model 8453 UV−visible spectrophotometer (Agilent Technologies).

Protein Production and Characterization. AarC expression plasmid pJK357 and AarCH6 expression plasmid pJK385 have been described previously.[28] The QuikChange II site-directed mutagenesis kit (Stratagene), plasmid template pJK385, and appropriate ODN pairs were used to create plasmids for the expression of AarCH6 mutants S71A (pJK564), R228E (pJK512), E294A (pJK513), N347A (pJK524), E435A (pJK514), E435D (pJK517), and E435Q (pJK516). Plasmid DNA sequenced in both directions by the staff of the Purdue University Genomics Core Facility contained the expected DNA sequences. Experimental details for AarC and AarCH6 production, isolation, and characterization by circular dichroism (CD) are given in the Supporting Information.

Steady-State Kinetic Analysis. Citrate synthase-dependent VisF/VisR assays and high-performance liquid chromatography (HPLC)-coupled LCF/LCR assays were performed as described previously,[28] except that the concentrations of enzymes and substrates and the durations of the reactions were adjusted as required for AarCH6 mutants. A unit is defined as the amount of enzyme that forms 1 μmol of product per minute.

Alternate carboxylate substrates (CoA acceptors) were identified using modified LCR assays containing 50 mM potassium phosphate (pH 8.0), 100 mM potassium chloride, 20 mM carboxylate (pH 8.0), 1 mM acetyl-CoA, and 5 μg of AarCH6. Aliquots (0.1 mL) were withdrawn prior to the addition of enzyme and 5 and 30 min after the addition of enzyme, quenched with 6.25% trichloroacetic acid (0.4 mL), vortexed briefly, and centrifuged at 16100*g* for 3 min. The soluble portion was transferred to an autosampler vial and analyzed by reverse-phase ion-pair HPLC. Compounds identified as alternate substrates were examined in saturation experiments employing modified LCR assays in which succinate was replaced by the candidate CoA acceptor.

CoA and CoA thioesters were resolved on a Breeze HPLC system (Waters) equipped with a Symmetry C18 column [4.6 mm × 75 mm, 3.5 μm (Waters)]. Acid-quenched reaction mixtures (25−100 μL) were applied using a 717plus autosampler (Waters). The column was developed at 30 °C and 0.8 mL min^{-1} with detection at 260 nm. A mixture of 200 mM sodium phosphate and 150 mM sodium acetate (pH 4.6) was used in a water/methanol solvent system. The gradient program was as follows: 4.5% methanol (isocratic) from 0 to 5 min, 4.5 → 15% methanol (linear gradient) from 5 to 15 min, 15% methanol (isocratic) from 15 to 17 min, 15 → 4.5% methanol (linear gradient) from 17 to 22 min, and 4.5% methanol (isocratic) from 22 to 27 min. The initial and final isocratic steps were performed in buffers without methanol for the analysis of reaction mixtures containing formate, glycolate, glyoxylate, oxalate, or tartrate, while the intermediate isocratic step was lengthened by 5 min for the analysis of reaction mixtures containing butyrate. Acyl-CoA peak areas were compared to an acetyl-CoA standard as described previously.[28]

Kinetic constants were obtained by nonlinear least-squares fitting to the Michaelis−Menten model, a substrate inhibition model (eq 1), or a competitive inhibition model (eq 2) using gnuplot 4.4. In these equations, K_i is an inhibition constant and C is the inhibitor concentration.

$$v = \frac{VS}{K_m + S\left(1 + \frac{S}{K_i}\right)} \quad (1)$$

$$v = \frac{VS}{S + K_m\left(1 + \frac{C}{K_i}\right)} \quad (2)$$

The ability of AarCH6 to process multiple substrates was quantitated by the substrate promiscuity index *I*, the relative probability of substrate conversion in an equimolar mixture of a set of alternative substrates, which ranges from 0 (perfect specificity, conversion of only one substrate) to 1 (perfect promiscuity, equal conversion of all substrates), and the weighted substrate promiscuity index *J*.[32] Weighting was based on the chemical diversity of the substrate set, enumerated using a list of 92 chemical descriptors that has been described previously.[32]

Crystallization and Data Collection. AarC and AarCH6 crystals were grown at room temperature (~22 °C) by the hanging drop vapor diffusion method. Reservoirs contained 0.5 mL of screening solution (Wizard I and II kits, Emerald BioSystems) supplemented with 25 mM 2-mercaptoethanol. Drops consisted of 2 μL of protein solution [5.6 mg mL^{-1} AarC in 45 mM potassium phosphate (pH 8.0), 90 mM potassium chloride, and 2 mM CoA or 6.0 mg mL^{-1} AarCH6 in 45 mM Tris-HCl (pH 8.0), 90 mM potassium chloride, and 2 mM CoA] and 2 μL of reservoir solution.

Orthorhombic crystals appeared in 0.8−1.0 M sodium citrate, 0.1 M imidazole (pH 8.2), and 25 mM 2-mercaptoethanol. Crystals were soaked in 15% (w/v) sorbitol, 1.1 M sodium citrate, 0.1 M imidazole (pH 8.2), 25 mM 2-mercaptoethanol, and 2 mM CoA for 24 h at room temperature prior to being flash-cooled by rapid immersion in liquid N_2.[33] Water, acetyl-CoA (2 mM), succinyl-CoA (2 mM), or dethiaacetyl-CoA (10 mM) was substituted for CoA in drops and cryoprotectants in an effort to obtain unliganded or alternate liganded structures. Crystals used for the trapping of covalent adducts were soaked in cryoprotectant solutions lacking ligand for 22 h, transferred to a cryoprotectant solution containing acetyl-CoA (2 mM) for 2 h, and flash-cooled.

Hexagonal crystals appeared in 1.7−2.0 M ammonium sulfate, 0.2 M sodium chloride, 0.1 M sodium cacodylate (pH 6.5), and 25 mM 2-mercaptoethanol. These crystals were processed as described above, except that the cryoprotectant consisted of 15% (w/v) sorbitol, 2.2 M ammonium sulfate, 0.25 M sodium chloride, 0.1 M sodium cacodylate (pH 6.5), 25 mM 2-mercaptoethanol, and 2 mM CoA.

X-ray diffraction data were collected at the Advanced Photon Source (Argonne National Laboratory, Argonne, IL). Diffraction data were indexed, integrated, and scaled in HKL2000.[34]

Determination and Refinement of Structure. The structure of the AarCH6·CoA·citrate complex (PDB entry 4eu7) was determined by molecular replacement using a threaded AarC model corresponding to a single subunit (residues 3−505 in GenBank entry ACD85596). The model was computed using SWISS-MODEL[35] based on coordinates from a biochemically uncharacterized CoA-transferase (PDB entry 2g39) from *Pseudomonas aeruginosa* that is 48% identical to AarC. All refinement steps were performed using PHENIX.[36] Automated building (PHENIX AutoBuild) was used to improve the initial model for AarCH6·CoA·citrate (PDB entry 4eu7) and AarCH6-S71A·CoA (PDB entry 4eu8) complexes. The subsequent early refinement procedure consisted of successive rounds of rigid-body refinement, simulated annealing, coordinate optimization, isotropic temperature factor refinement, and automated water picking. Later rounds of refinement consisted of coordinate optimization, isotropic temperature factor refinement, and automated water picking. Noncrystallographic symmetry (NCS) restraints were applied for automated building of the AarCH6·CoA·citrate (PDB entry 4eu7) model and for all stages of the refinement of the AarCH6·CoA (PDB entry 4eu4), AarCH6-R228E·CoA (PDB entry 4eu9), and AarCH6-E294A·dethiaacetyl-CoA (PDB entry 4euc) models. Manual building and water addition were conducted using Coot[37] after each round of automated refinement. Ligand coordinates and restraints were obtained from HIC-Up[38] and modified using PHENIX.

All other AarC(H6) structures were determined by molecular replacement using the refined coordinates of the AarCH6·CoA·citrate complex (PDB entry 4eu7, chain A, residues 2−514) as the search model.

All structural images were generated with PyMOL.[39] Electrostatic potential maps were computed using the PDB2PQR[40] web server (pH 7 and 298 K) and the APBS[41] plugin for PyMOL.

Ligand Conformation Calculations. Michaelis complexes and the glutamylsuccinyl anhydride adduct were manually constructed in active sites containing the crystallographically observed acetylglutamyl anhydride or glutamyl-CoA thioester intermediates [both of which are present in the AarCH6·-CoA·acetate complex (PDB entry 4eu6)]. A single water (HOH517) and all residues (Phe35, Thr36, Ala70, Ser71, Phe92, Leu114, Gln267, Gly269, Val270, Glu294, Val295, Asn361, Gly387, Gly388, and Ser389) that directly contacted modeled atoms were included during building and subsequent energy minimization. Hydrogen atoms were added in appropriate riding positions before equilibrium conformer calculations incorporating a Monte Carlo search method (5000 K) and MMFF94 force field were performed. Only the positions of hydrogen atoms and modeled non-hydrogen atoms were refined during energy minimization. All non-hydrogen protein atoms and selected ligand atoms were "frozen". Corrections for implicit solvent were not applied at any point during refinement. All molecular mechanics calculations were performed with Spartan '02 (Wavefunction).

RESULTS

Protein Production, Isolation, and Biophysical Characterization. AarC was purified to near-homogeneity using a procedure involving ammonium sulfate fractionation, gel-filtration chromatography, ion-exchange chromatography, and dye-affinity chromatography (Table S2 of the Supporting Information). Kinetic analysis of AarC (Figure S1 of the Supporting Information) yielded steady-state kinetic constants for acetate saturation [k_{cat} = 290 ± 30 s^{-1}, K_m = 110 ± 20 mM, k_{cat}/K_m = (2.6 ± 0.5) × 10^3 M^{-1} s^{-1}, and K_i = 1600 ± 500 mM] that are similar to those reported for AarCH6,[28] indicating that the C-terminal fusion in AarCH6 does not interfere with catalysis. (As previously discussed,[28] high acetate K_m values are physiologically reasonable in *A. aceti*.)

Heterologously overproduced AarC(H6) was ~90% insoluble,[28] even when the C41(DE3) expression host[42] or lower expression temperatures[43] were employed. A ~10-fold increase in the yield of soluble AarCH6 was observed when AarCH6 was co-overproduced with *Escherichia coli* GroES and GroEL, which are presumed to function as folding aides.[29] Wild-type (wt) and mutant AarCH6 forms were routinely co-overproduced with GroESL and purified to near-homogeneity

dx.doi.org/10.1021/bi300957f | *Biochemistry* 2012, 51, 8422−8434

using the same procedure. GroESL co-overproduction failed to ameliorate the complete insolubility of AarCH6-E435A and AarCH6-E435Q.

ESI-TOF-MS analysis was consistent with 504-residue (AarC) or 513-residue (wt and mutant AarCH6) proteins lacking Met1 (Table S3 of the Supporting Information).

The diminution of CD signal intensity was used to monitor the thermal unfolding of AarC and AarCH6 as a function of pH (Figure S4 of the Supporting Information). The stability of each protein decreased sharply as the pH approached 3.8. AarC remained folded under physiological conditions encountered in the acidic cytoplasm (pH 3.8−6.8)[44] of the relatively thermophilic (≤35 °C) strain *A. aceti* 1023[22,23] but seems to be less stable at pH ≤4 than other characterized *A. aceti* proteins.[25,45,46] AarCH6 was somewhat less stable than AarC, but only under low-pH conditions that would likely result in the protonation of surface-exposed histidine residues in the affinity tag.

Substrate Spectrum. Interception of the glutamyl-CoA thioester adduct by noncognate carboxylates accounts for the substrate promiscuity attributed to many CoA-transferases. All of the carboxylates that supported detectable AarCH6 activity were ≥10-fold poorer substrates than the physiological substrates acetate and succinate (Table 1). Lower k_{cat} values for nonphysiological substrates accounted for most of the difference (Table S4 of the Supporting Information), while many K_m values were comparable to that determined for acetate.

Table 1. Alternate Substrates for AarCH6[a]

carboxylate	relative k_{cat}/K_m (%)
succinate	100
acetate[b]	5.1
acetoacetate[b]	0.35
propionate	0.34
D-malate	0.28
fumarate	0.20
L-malate	0.10[c]
formate	0.033
oxaloacetate	0.011
DL-methylsuccinate	0.010
glutarate	0.0012

[a]Full details are given in Table S4 of the Supporting Information. No activity (≤0.01 unit/mg) was detected with glycolate, glyoxylate, oxalate, trifluoroacetate, DL-lactate, L-lactate, malonate, pyruvate, maleate, butyrate, D-tartrate, L-tartrate, α-ketoglutarate, citrate, or DL-isocitrate. Acetyl-CoA was the CoA donor except where noted. [b]Succinyl-CoA was the CoA donor. [c]Combined activity for two products that are presumed to be regioisomers.

A pattern consistent with weak competitive inhibition against succinate (K_i = 150 mM) was observed in LCR assays modified by the addition of citrate (Figure S5 of the Supporting Information). Citrate is not an AarCH6 substrate, nor is it capable of inducing acetyl-CoA hydrolysis.

Qualitatively, AarCH6 appears to have greater fidelity and higher catalytic activity than other characterized class I CoA-transferases.[7,14,47−50] Substrate promiscuity indices, I = 0.12 and J = 0.32 for AarCH6 with the substrate set examined, indicate a moderate level of promiscuity (Tables S5−S7 of the Supporting Information).

Crystal Structures of AarC and AarCH6. Two AarCH6 crystal forms were identified by sparse-matrix screening: bipyramidal hexagonal crystals that appeared in solutions containing ammonium sulfate and clusters of thin orthorhombic crystals that appeared in solutions containing sodium citrate (Figure S6 of the Supporting Information). Faster crystallization of both forms was noted for AarCH6 co-overproduced with GroESL and subsequently gel-filtered. Orthorhombic crystals gave X-ray diffraction patterns extending beyond 2.0 Å. In contrast, the larger hexagonal crystals failed to yield X-ray diffraction data extending beyond 2.8 Å. Hexagonal crystals soaked in a cryoprotectant solution for <24 h produced diffraction patterns with dark ice rings.

A structure of AarCH6 bound to CoA and citrate (PDB entry 4eu7) was obtained from an orthorhombic crystal by molecular replacement and refined to a model with good statistics (Table 2). The sole Ramachandran outlier in most chains, Pro91, was modeled into excellent electron density. The asymmetric unit contained the expected biological dimer of subunits, each with a topology (Figure S7 of the Supporting Information) similar to those of other class I CoA-transferases.[51]

Table 2. Summary of Crystallographic Results[a]

PDB entry	protein	ligand(s)	resolution (Å)	R_{cryst}[b]	R_{free}[c]
4eu3	wt	none[d]	1.58	0.156	0.189
4eu4	wt	CoA	2.80	0.178	0.223
4eu5	wt	CoA	1.74	0.167	0.209
4eu6	wt	CoA, acetate[e]	1.99	0.164	0.209
4eu7	wt	CoA, citrate	1.70	0.156	0.194
4eu8	S71A	CoA	1.81	0.180	0.226
4eu9	R228E	CoA	1.48	0.157	0.179
4eua	R228E	CoA	2.40	0.152	0.209
4eub	E294A	CoA	1.97	0.154	0.209
4euc	E294A	dethiaacetyl-CoA	2.64	0.168	0.225
4eud	no tag	CoA, citrate	1.95	0.159	0.206

[a]All proteins crystallized in space group $P2_12_12_1$, except for PDB entry 4eu4, which crystallized in space group $P6_222$. Tables S8−S11 of the Supporting Information contain a complete set of X-ray data collection and refinement values. [b]$R_{cryst} = \sum|F_o - \langle F_c\rangle|/\sum F_o$, where the summation is over the data used for refinement. [c]R_{free} is defined in the same way as R_{cryst} but was calculated using the 5% of the data that were excluded from refinement. [d]The active site of subunit B contains citrate. [e]Acetylglutamyl anhydride (subunit A) and glutamyl-CoA thioester (subunit B) adducts are also present.

The AarC(H6) monomer is composed of distinct N- and C-terminal domains, each displaying an open α/β-fold (Figure 2). The domains are joined by two rigid loops (residues 171−178 and 182−215) that depart from the N-terminal domain to add strand β8 to the core C-terminal β-sheet and a flexible domain linker (residues 224−235) that spans a deep, funnel-shaped cleft. The active-site glutamate (Glu294) is located at the bottom of the cleft. The positively charged active-site region is encircled by a negatively charged zone. Other regions on the AarC surface appear to be largely neutral (Figure S9A−C of the Supporting Information).

The extensive, highly hydrated monomer−monomer interface buries 3500 Å^2 of surface area per subunit (17% of the total surface area). Four chloride ions are present at the interface, associated with buried and otherwise uncompensated arginine residues from each monomer (Arg120 and Arg354). When

dx.doi.org/10.1021/bi300957f | Biochemistry 2012, 51, 8422−8434

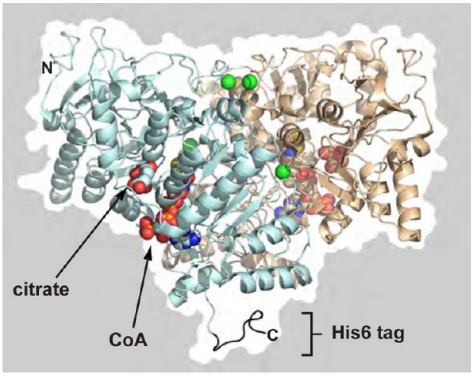

Figure 2. Crystal structure of the AarCH6·CoA·citrate complex (PDB entry 4eu7). AarCH6 is a dimer with four chloride ions (green spheres) at the monomer−monomer interface. CoA and citrate are bound in a deep, funnel-shaped active-site cleft between the N- and C-terminal domains of each subunit. The molecular surface is depicted in silhouette with the pseudo-2-fold axis lying vertical in the plane of the page.

these ions were modeled as water molecules, the resulting *B* factors were substantially lower than those of surrounding protein atoms and residual density remained in the σA-weighted $mF_o - DF_c$ difference map. Weak anomalous density centered around each chloride ion (PDB entry 4eua) provided direct evidence of a third-row element at these positions (Figure S8 of the Supporting Information). Given the buried locations of Arg120 and Arg354 and the lack of nearby negatively charged residues, the four chloride ions appear to be important for AarC(H6) dimerization.

Hexagonal AarCH6 crystals also contained an asymmetric unit corresponding to the biological dimer (PDB entry 4eu4). These crystals had higher solvent content and diffracted to lower resolution (Table S8 of the Supporting Information) but had reasonable packing interactions among asymmetric units. The orthogonal and hexagonal structures had no significant differences (Cα rmsd = 0.54 Å for residues 2−505), which suggests that crystal packing interactions do not significantly perturb the structure of AarCH6.

AarCH6 that crystallized in the orthorhombic lattice regularly possessed a complete and ordered hexahistidine tag (residues 506−514) in subunit A, forming a 3_{10}-helix that is involved in crystal packing interactions with an adjacent asymmetric unit. Ordered hexahistidine tags are rare and are often attributed to stabilizing packing contacts,[52] which are lacking for subunit B in the orthorhombic lattice and both subunits in the hexagonal lattice, neither of which showed density corresponding to the tag. Orthorhombic AarC·CoA·citrate crystals (PDB entry 4eud) displayed no significant structural differences relative to the same complex formed with AarCH6 (PDB entry 4eu7; Cα rmsd = 0.17 Å for residues 2−505), which suggests that the addition of a hexahistidine tag does not significantly perturb the structure of AarC. All other wt and mutant AarCH6 structures were determined from orthorhombic crystals (Table S8 of the Supporting Information).

CoA and Citrate Binding. Electron density consistent with CoA and citrate was observed in the funnel-shaped cleft between the N- and C-terminal domains of AarCH6 [PDB entry 4eu7 (Figure 3A)]. With the exception of a single hydrophobic interaction, CoA contacts only residues in the C-terminal domain. The adenine moiety is located in a

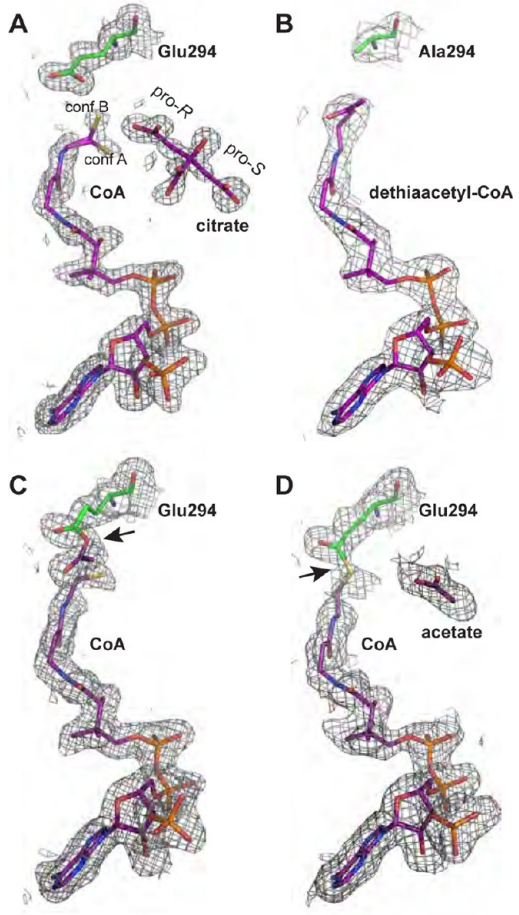

Figure 3. Electron density corresponding to bound ligands. Each panel contains a σA-weighted $2mF_o - DF_c$ map, calculated with Glu294 or Ala294 and ligands omitted, with a 2 Å carve radius. Adduct attachment points are indicated with arrows. (A) AarCH6·CoA·citrate complex (PDB entry 4eu7, subunit B) contoured at 1.0σ. The thiolate moiety of CoA is modeled in two conformations (conf A and conf B). (B) AarCH6-E294A·dethiaacetyl-CoA complex (PDB entry 4euc) contoured at 1.0σ. (C) Acetylglutamyl anhydride adduct of the AarCH6·CoA·acetate complex (PDB entry 4eu6, subunit A) contoured at 0.9σ. An alternate view of the electron density in this active site is provided in Figure S11 of the Supporting Information. (D) Glutamyl-CoA thioester adduct of the AarCH6·CoA·acetate complex (PDB entry 4eu6, subunit B) contoured at 0.6σ.

hydrophobic pocket near the entrance to the cleft, while the pantetheine arm extends deeply into the active site, terminating near Glu294. Citrate contacts only residues in the N-terminal domain and the domain linker, forming extensive polar contacts with the side chains of Ser71, Thr94, and Arg228. While citrate is not an AarCH6 substrate (Table S4 of the Supporting Information), its resemblance to succinate and acetate suggests that this region might bind one or both physiological carboxylate substrates. However, the large gap between citrate and Glu294 (>7 Å) appears to eliminate the possibility that the citrate binding site is the site of acetate or succinate binding in either Michaelis complex.

Protein Conformational Dynamics. AarCH6 was observed in several distinct conformations ranging from fully open to fully closed (Figure 4). The active site in the fully open conformation is readily accessible to acyl-CoA substrates. Interactions with the CoA moiety trigger a progressive constriction that can be envisioned to occur in three stages.

dx.doi.org/10.1021/bi300957f | *Biochemistry* 2012, 51, 8422−8434

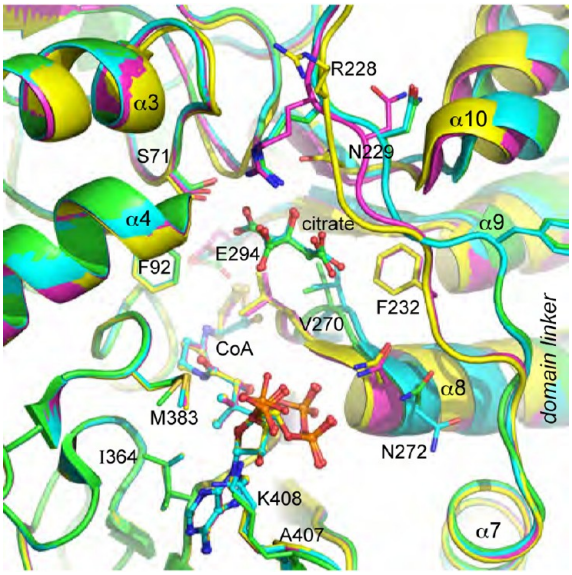

Figure 4. Stepwise constriction of AarCH6. The funnel-shaped AarCH6 active-site cleft narrows upon binding CoA. The cleft opening is in the foreground, and the cleft base, defined by Glu294, is in the background. Residues in the fully open conformation are colored green (PDB entry 4eu3), residues in the mostly open conformation are colored cyan (PDB entry 4eu7), residues in the mostly closed conformation are colored purple (PDB entry 4eu5), and residues in the fully closed conformation are colored yellow (AarCH6-E294A, PDB entry 4eub). CoA and citrate from all models are depicted in ball-and-stick representation. All are from subunit B of the indicated structures.

In the first stage, the active site remains largely open, but small, local structural shifts improve hydrogen bonding, electrostatic, and hydrophobic interactions with the adenine and ribose rings, the 3′-phosphate, and the β-alanyl oxygen [O7″, acyl-CoA numbering[53] given in Figure 5 (Figure S10A of the Supporting

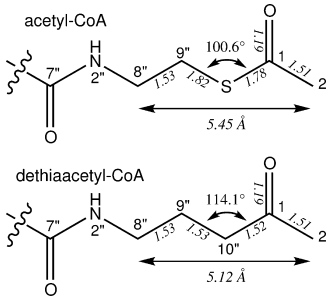

Figure 5. Acetyl-CoA and the nonhydrolyzable analogue dethiaacetyl-CoA are nearly isosteric except for altered geometries in the vicinity of the atomic substitution. Indicated interatomic distances (in italics, angstroms) and angles are based on equilibrium geometries computed using the Hartree−Fock model and a 6-31G* basis set for ethyl thioacetate (top) and 2-pentanone (bottom). Atom numbering follows a previously described scheme for acyl-CoAs.[53]

Information)]. In the second stage, the active site shrinks substantially. Helices α8−α11 and the loop connecting β10 and α8 translate toward CoA to maximize hydrogen bonding and electrostatic interactions with the diphosphate moiety and the adjacent pantoate C3″ hydroxyl group. The concomitant relocation of Val270 creates a catalytic pocket, defined by hydrophobic residues Phe35, Thr36, Ala70, Phe92, Leu114, and Val295, that isolates the catalytic glutamate and CoA thiol(ate) from bulk solvent. An accompanying rotation of the domain linker places the side chain of Phe232 between α9 and the mobile loop connecting β10 and α8. In the final stage, continued rotation of the domain linker toward the N-terminal domain pushes the side chain of Asn229 into the active site while pulling the side chain of Arg228 onto the protein surface, effectively removing the citrate binding site. Mobile regions near the active site have relatively high *B* factors, consistent with multiple conformations in the crystal.

CoA adopts a very similar conformation in most structures, except for the thiolate moiety, which rotates inward as the enzyme closes (Figure 4). The CoA C7″−N2″−C8″−C9″ dihedral angle is −106° (major conformer; −115° for the minor conformer) in the mostly open conformation (PDB entry 4eu7), −170° in the mostly closed conformation (PDB entry 4eu5), and 177° in the fully closed conformation (PDB entry 4eub). This progression suggests that enzyme closure constrains the acyl-CoA thioester in a near-attack configuration.

Complexes Formed from Acyl-CoA Substrates or Dethiaacetyl-CoA. Attempts to cocrystallize AarCH6 with acetyl-CoA (or succinyl-CoA) failed to yield covalent anhydride and CoA thioester intermediates that are characteristic of the class I CoA-transferase reaction (Figure 1), probably because of the short half-lives of the thioester substrates at pH 8 [~10 h (E. A. Mullins, unpublished observations)]. However, covalent adducts with Glu294[a] were detected by freeze-trapping an AarCH6 crystal soaked with acetyl-CoA (PDB entry 4eu6). Subunit A contains the acetylglutamyl anhydride adduct and CoA thiolate (Figure 3C and Figure S11 of the Supporting Information). Subunit B contains acetate, bound to the side chains of Ser71, Thr94, and Arg228, and the glutamyl-CoA thioester adduct (Figure 3D). Acetate occupies the same site as the pro-*R* acetyl moiety of citrate (PDB entry 4eu7), which is too remote from Glu294 to represent a Michaelis complex binding site. The only known source of acetate is acetyl-CoA hydrolysis, possibly in the adjacent catalytic pocket. The CoA conformation is the same in both freeze-trapped adducts, except for an outward rotation of the thiolate moiety in the anhydride form (C7″−N2″−C8″−C9″ dihedral angle of −161°, compared to 167° in the glutamyl-CoA thioester). In this conformation, the CoA thiolate is 3.4 and 3.2 Å from the internal and external carbonyl carbons of the acetylglutamyl anhydride, respectively, and stabilized by hydrogen bonding interactions with Val270 NH and HOH517.

AarCH6-E294A was cocrystallized with dethiaacetyl-CoA,[54] a competitive inhibitor of AarCH6 that closely resembles acetyl-CoA and binds with a K_d of 0.8 μM.[28] Each active site in the resulting structure (PDB entry 4euc) contains dethiaacetyl-CoA in a nearly identical conformation (Figure 3B). The dethiaacetyl-CoA "acetyl" group curves back toward the pantoate moiety so that the ketone O1 atom forms hydrogen bonds to dethiaacetyl-CoA N2″ and Gly388 NH (2.55 Å average O1−N distance). The dethiaacetyl-CoA C7″−N2″−C8″−C9″ dihedral angle (171°) is close to that in the glutamyl-CoA thioester (PDB entry 4eu6, subunit B). When superposed on a wt structure, dethiaacetyl-CoA C1 would be ~2 Å from the nearest Glu294 carboxylate oxygen, with an O−C1−O1 angle of 113°. This arrangement should allow acetyl-CoA to adopt a near-optimal configuration for nucleophilic attack by Glu294[55] and to form two hydrogen bonds that stabilize the oxyanion of the resulting tetrahedral intermediate.

dx.doi.org/10.1021/bi300957f | *Biochemistry* 2012, 51, 8422−8434

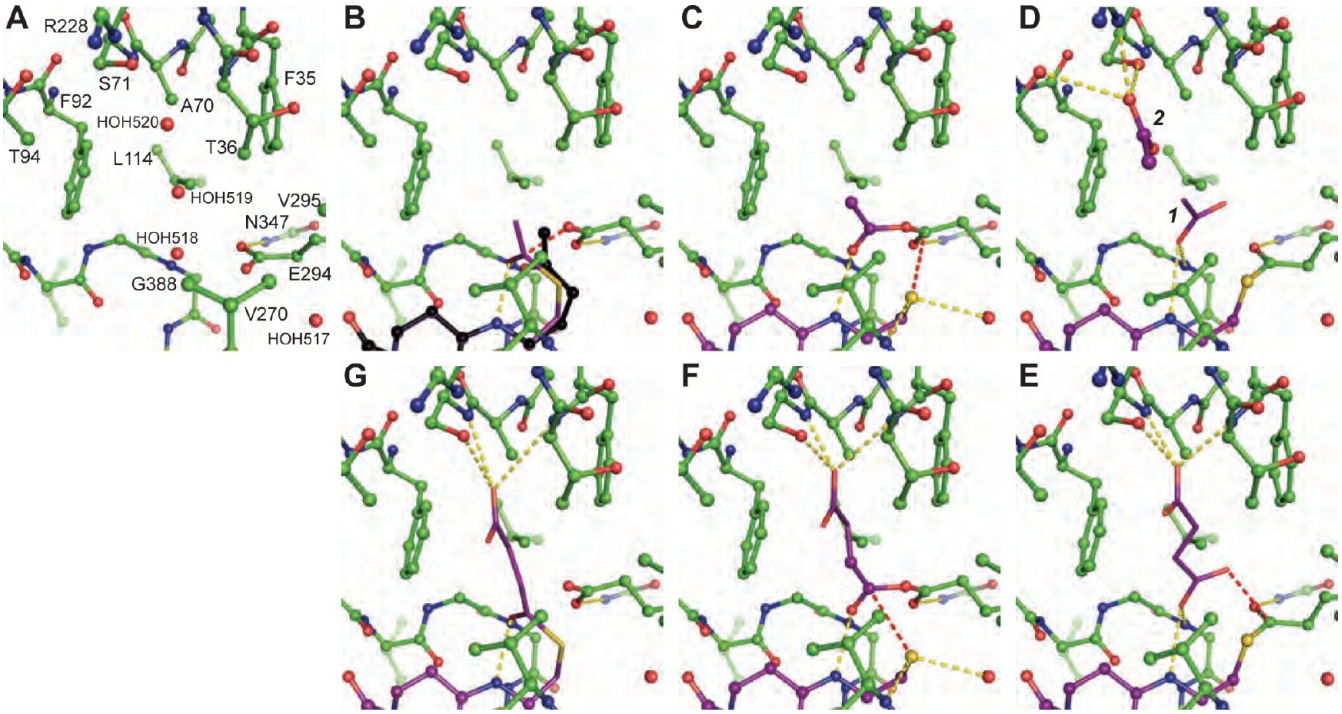

Figure 6. Structural depiction of the SCACT reaction, illustrated in the reverse biosynthetic direction (acetyl-CoA + succinate → acetate + succinyl-CoA). Crystallographically observed intermediates (ball-and-stick representation) and modeled intermediates (stick representation) were combined to produce a complete structural description of the SCACT mechanism. (A) Unliganded. (B) Acetyl-CoA complex. The acetyl-CoA analogue dethiaacetyl-CoA is colored black. (C) Acetyl anhydride adduct and CoA thiolate. (D) CoA thioester adduct and acetate. Acetate is depicted in two positions. Position 2 outside the catalytic pocket was crystallographically observed (Figure 3C), and position 1 inside the catalytic pocket was modeled. (E) CoA thioester adduct and succinate. (F) Succinyl anhydride adduct and CoA thiolate. (G) Succinyl-CoA complex. HOH518, HOH519, and HOH520 (panel A) are displaced by the acyl/carboxylate moieties (except in panel D, model 2). Modeled intermediates were manually positioned within the active site, and equilibrium conformations were determined using molecular mechanics calculations. Atoms shown in ball-and-stick representation were either frozen or omitted during optimization. Yellow and red dotted lines indicate hydrogen bonds and possible paths of nucleophilic attack, respectively.

Model Building. Models for missing reaction intermediates were built using closely related crystallographic observations as starting points. All were manually built prior to geometrical optimization of a small number of atoms. In all cases, the polar and hydrophobic contacts present in manually built models were retained in the geometrically optimized final models (Figure 6).

A model for the glutamylsuccinyl anhydride adduct [model F (Table S15 of the Supporting Information)] was based on the acetylglutamyl anhydride adduct (PDB entry 4eu6, subunit A). A carboxymethyl group was appended to the acetyl anhydride to create a fully extended succinyl anhydride. This conformation allowed the distal carboxylate to form hydrogen bonding interactions with Thr36 NH and Ser71 O^{γ} and NH. The optimized model made hydrophobic contacts with the side chains of Phe35, Thr36, Ala70, Phe92, Leu114, Val270, and Val295 and retained a nearly trans geometry.

A model for the acetyl-CoA Michaelis complex [model B (Table S12 of the Supporting Information)] was based on the dethiaacetyl-CoA complex (PDB entry 4euc). Hydrogen bonding interactions with Gly388 NH and CoA N2″ were retained. The only significant alterations in the optimized model were associated with the replacement of methylene C10″ with sulfur (Figure 5). (Acetyl-CoA C1 is ~2 Å from the nearest Glu294 carboxylate oxygen, with an O−C1−O1 angle of ~110°.) A model for the succinyl-CoA Michaelis complex [model G (Table S16 of the Supporting Information)] was based on model B and altered to contain the succinyl moiety from model F in the place of the acetyl moiety.

Models for the Michaelis complexes containing acetate [model D1 (Table S13 of the Supporting Information)] or succinate [model E (Table S14 of the Supporting Information)] were built adjacent to the observed glutamyl-CoA thioester complex (PDB entry 4eu6, subunit B). Atoms from the acyl moieties in the corresponding anhydride adducts (PDB entry 4eu6, subunit A and model F, respectively) were used to manually construct the models. The optimized models retained the hydrogen bonding interactions and hydrophobic contacts made by the anhydride adducts.

Structural Comparisons and Phylogenetic Analyses. Paralogous groups within the class I CoA-transferase superfamily have diverse subunit and domain arrangements consistent with low levels of sequence identity between groups. Each group contains one or more enzyme families that recognize different pairs of acyl-CoA and carboxylate substrates. However, the superfamily is mechanistically homogeneous (Figure 1), and its members have related backbone topologies that conserve the three-dimensional arrangement of the four key catalytic residues. Structural alignments (Figure 7A and Table S17 of the Supporting Information) show that Glu294, Asn347,[b] and Gly388 homologues maintain a fixed relative orientation in diverse class I CoA-transferases. Val270 homologues were crystallized in different locations along the path this residue traverses as the enzyme closes.

dx.doi.org/10.1021/bi300957f | *Biochemistry* 2012, 51, 8422−8434

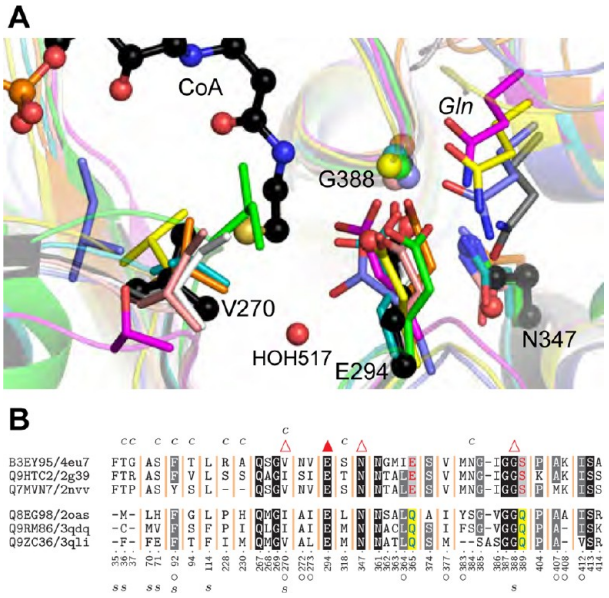

Figure 7. Comparisons of class I CoA-transferase sequence and structure. (A) Constellation of conserved active-site residues in 10 phylogenetically diverse class I CoA-transferases. AarC side chains and ligands are depicted in ball-and-stick representation. The isolated red sphere indicates a solvent atom located at a conserved location in structures determined at sufficiently high resolution [HOH517 in AarC(H6) structures]. Carbon atoms and ribbons are colored by PDB entry: 4eu7 (AarCH6), black; 2nvv, teal; 2g39, green; 2oas, white; 3gk7,[59] salmon; 3oxo,[15] slate; 3qli,[74] orange; 2ahv,[14] yellow; 1k6d,[82] gray; 1poi,[51] magenta. Residue numbers, sequence accession codes, and protein functional data are given in Tables S17 and S18 of the Supporting Information. (B) Residues located near ligands in the AarCH6·CoA·citrate complex (PDB entry 4eu7). A partial structure-based sequence alignment highlights residues involved in enzyme chemistry (red triangles), including the covalent attachment point Glu294 (filled triangle), or that are part of the binding site for citrate (*c*), succinate or the acyl group of succinyl-CoA (*s*), or CoA (○). Absolutely conserved residues are shown with black backgrounds. Differentially conserved residues are shown with colored letters. The full alignment is given in Figure S13 of the Supporting Information.

Phylogenetically diverse bacteria contain AarC paralogues [SCACT group (Figure 7B and Figure S12 of the Supporting Information)]. Biochemically characterized members of this group recognize succinate/succinyl-CoA and are able to perform the SCACT reaction.[28,48,56,57] AarC residues with important roles in catalysis, structure, CoA binding, or interactions with the distal carboxylate in succinate/succinyl-CoA models are highly conserved in the SCACT group. AarC residues that interact with citrate are not widely conserved.

Structure-based sequence alignments, performed as described in the Supporting Information, were used to identify proteins that closely resemble AarC but have different substrate preferences. The SCACT group is highly similar in structure and sequence to the 4-hydroxybutyrate CoA-transferase (4HBCT) group (Figure 7B,C). However, succinate is not a substrate for *Clostridium aminobutyricum* 4HBCT,[58] which suggests that residues involved in recognizing distal portions of the C4 substrate are different in the SCACT and 4HBCT groups. AarC residues with important roles in catalysis, structure, or CoA binding are highly conserved in the 4HBCT group, but those that interact with the distal carboxylate in succinate/succinyl-CoA models are not. In *C. aminobutyricum* 4HBCT, the side chain of His31 has been proposed to form a hydrogen bond to the substrate γ-hydroxyl moiety.[59] The corresponding AarC residue is Gly34. AarC residues that interact with citrate are not conserved in the 4HBCT group.

Kinetic and Structural Characterization of AarCH6 Mutants. Several soluble AarCH6 mutants were kinetically (Table 3 and Table S19 of the Supporting Information) or structurally (Table 2) characterized.

Table 3. Kinetic Data for AarCH6 Mutants[a]

	k_{cat}/K_m (mM^{-1} s^{-1})		k_{cat}/K_m (μM^{-1} s^{-1})	
AarCH6 form[b]	acetate	succinate	acetyl-CoA	succinyl-CoA
wt[c]	4	79	3.4	9
S71A	0.029	0.030	0.7	0.074
R228E[d]	0.6	0.3	2.3[e]	0.13[e]
E294A[f]	~0	~0	~0	~0
N347A	0.16	2.7	0.7	0.39
E435D	3	73	5.2	9

[a]Table S19 of the Supporting Information contains a full set of kinetic parameters for each enzyme form with detectable catalytic activity. [b]Activity measurements could not be performed for the insoluble AarCH6-E435A and AarCH6-E435Q mutants. [c]From ref 28. [d]AarCH6-R228E could not be fully saturated with either carboxylate substrate. Values were estimated from the initial slopes of the substrate saturation plots (Figure S18 of the Supporting Information). [e]Acyl-CoA kinetic parameters were determined at subsaturating, fixed concentrations of succinate (550 mM) or acetate (750 mM). [f]AarCH6-E294A did not support activity above the estimated ~0.009 s^{-1} detection limit.

Glu294 is the highly conserved site of covalent catalysis in class I CoA-transferases. Mutations at this position have either obliterated catalytic activity or caused aberrant thioesterase activity.[59,60] Introduction of a Glu294 → Ala mutation into AarCH6 reduced the specific activity by >10000-fold. A crystal structure of AarCH6-E294A shows no structural alterations apart from a slight inward rotation of Thr36 (PDB entry 4eub).

Glu435 is conserved throughout class I CoA-transferases. Its location outside the active-site cleft, in a conserved β-hairpin motif, is inconsistent with an early proposal that it plays a role in covalent catalysis in AarC.[60] The catalytic properties of AarCH6-E435D are nearly equivalent to those of wt AarCH6, while E435A and E435Q mutants are completely insoluble. Glu435 appears to have an important but purely structural role.

Asn347 is conserved in many class I CoA-transferases and has been proposed to orient the key glutamate side chain for nucleophilic attack[14] or stabilize oxyanion intermediates formed on the internal carbonyl.[51] AarCH6-N347A had impaired catalytic activity, but the apparent affinities for all four substrates were largely unaffected. These findings are consistent with a defect in catalysis that could arise from disruption of either or both of its proposed roles.

Ser71 is highly conserved within the SCACT group but not in other class I CoA-transferases (Figure S13 of the Supporting Information). In AarCH6 structural models, Ser71 makes polar side chain contacts to the distal carboxylate of succinate (Figure 6E−G). Ser71 also forms part of the citrate binding site, interacting with the same pro-*R* carboxylate oxygen that contacts Arg228 NH2.

AarCH6-S71A had impaired catalytic activity associated with lower k_{cat} values. A crystal structure of the AarCH6-S71A·CoA complex (PDB entry 4eu8) revealed that disruption of the three

dx.doi.org/10.1021/bi300957f | *Biochemistry* 2012, 51, 8422−8434

hydrogen bonds involving Ser71 induced a partial collapse of the catalytic pocket, in a region that would appear to be necessary to accommodate succinate and possibly acetate (Figure S16 of the Supporting Information). In one subunit, a shift also occurred in a surface-exposed unit of the N-terminal domain (Figure S17 of the Supporting Information).

Arg228 is found in only AarC and several closely allied SCACT group sequences (red taxa in Figure S12 of the Supporting Information). As described above, Ser71 and Arg228 interact with each other and with acetate or citrate in the auxiliary binding site outside the catalytic pocket. Arg228 is initially displaced from the active-site cleft as the enzyme constricts around acyl-CoA (PDB entry 4eub) but returns to allow partial reopening and carboxylate exchange from the glutamyl-CoA thioester adduct.

AarCH6-R228E was not saturated at a concentration of 0.5 M of either physiological carboxylate substrate (Figure S18 of the Supporting Information). An acetyl-CoA saturation curve with a normal shape, obtained at the highest achievable succinate concentration, furnished a specificity constant comparable to that of wt AarCH6, indicating AarCH6-R228E had a specific defect in its ability to bind both carboxylate substrates. (A modest defect in succinyl-CoA binding cannot be ruled out.)

Crystallographic analysis of AarCH6-R228E (PDB entry 4eu9) showed that the side chain of Glu228 is well-ordered and is displaced from the citrate binding region (Figure S14 of the Supporting Information). Nonetheless, the charge-reversed mutation diminishes the positive electrostatic potential in the active-site cleft (Figure S9 of the Supporting Information). A lower affinity for carboxylate substrates could be the result of diminished electrostatic attraction to the active-site cleft, disruption of a carboxylate binding function within the auxiliary binding site, perturbation of the conformational equilibrium, or a combination of multiple effects. Several carboxylates with charge-reversed distal moieties (e.g., 4-aminobutyrate) were not accepted as substrates by AarCH6-R228E (data not shown).

DISCUSSION

The kinetic mechanism and covalent intermediates of the archetypal class I CoA-transferase SCOT were established more than 35 years ago.[2,3,5−8] Subsequent studies predicted that protein conformational changes driven by substrate binding[7,8] allow enzyme−substrate interactions remote from the site of chemistry[9−11] to contribute to catalytic accelerations.[16] Crystal structures of AarC supplemented with conservative models illustrate how class I CoA-transferases use binding energy to induce a conformational change that accelerates elegant tandem acyl transfer reactions and to select for appropriate acyl-CoA and carboxylate substrates (Figure 6).

Mechanistic Strategies Used by AarC and Other Class I CoA-Transferases. The structural data presented here are consistent with the Jencks model for catalysis by class I CoA-transferases.[16] Acyl-CoA binding leads to the assembly of an oxyanion hole for the first tetrahedral intermediate (Figure 8A), a case of the "gear-shift" type[61] of induced fit between the enzyme and substrate.[62] As the active site constricts, the acyl-CoA (represented by dethiaacetyl-CoA) adopts a curled conformation, observed here for the first time, that is clamped against the nucleophilic glutamate carboxylate in an orientation suitable for nucleophilic attack. During this process, Glu294 shifts slightly and a rotation around the acyl-CoA C8″−C9″ bond places the thioester oxygen into a preorganized oxyanion

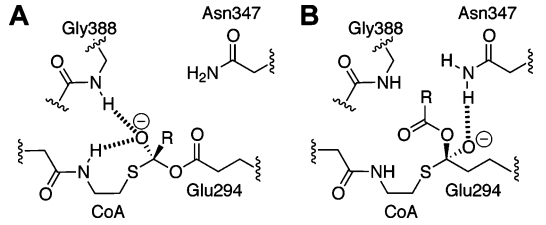

Figure 8. Stabilization of tetrahedral oxyanion intermediates within the AarCH6 active site. (A) Intermediate formed by the attack of Glu294 on the acyl-CoA carbonyl (Figure 6, B → C) and by the attack of CoA thiolate on the external carbonyl of the mixed anhydride adduct (F → G). (B) Intermediate formed by the attack of CoA thiolate on the internal carbonyl of the mixed anhydride adduct (C → D) and by the attack of the carboxylate substrate on the glutamyl thioester carbonyl (D → E).

hole. This restrictive conformation places the reacting atoms in a Bürgi−Dunitz configuration[55] suitable for attack by the *syn* orbital of the carboxylate[63] and exerts strain that would be relieved in the tetrahedral oxyanion intermediate and transition state.[7] In the modeled acetyl-CoA Michaelis complex, the Glu294 carboxylate oxygen and thioester carbonyl carbon atoms are in van der Waals contact. The same CoA conformation is observed in complexes containing dethiaacetyl-CoA, the acetylglutamyl anhydride adduct, and the glutamyl-CoA thioester adduct, which means minimal motion is required for the conversion of an acyl-CoA Michaelis complex to a carboxylate Michaelis complex (Figure 6, panels B → D and G → E). Previous studies of on-enzyme equilibria indicate that the acylglutamyl anhydride adduct may be less stable than the glutamyl-CoA thioester adduct.[6,7,9] Trapping of the acetylglutamyl anhydride adduct (Figure 3C and Figure S11 of the Supporting Information) suggests that anhydride cleavage is suppressed within the crystalline environment.

Acylglutamyl anhydride adduct thiolysis occurs at two carbonyls separated by only 2.5 Å, performed by two regions of the catalytic pocket that (arguably) represent separate active sites. These reactions are facilitated by discrete external and internal oxyanion holes that work together (Figure 8). The leaving group potential of the carboxylate product, formed by thiolysis of the internal anhydride carbonyl, is increased by interactions with CoA N2″ and Gly388 NH [the external oxyanion hole, serving a different function (Figure 6D, position 1)]. The leaving group potential of Glu294, formed by thiolysis of the external anhydride carbonyl, is increased by interactions with Asn347 N^{δ} [the internal oxyanion hole, serving a different function (Figure 6G)]. The leaving group potential of the CoA thiolate expelled by thioester cleavage is increased by interactions with Val270 NH and HOH517 (Figure 6C,F). Protein conformational changes triggered by acyl-CoA binding preorganize Val270 NH and CoA N2″ appropriately. With these hydrogen bond donors in their proper places, the enzyme can perform both reactions without much substrate motion, using the adjacent oxyanion holes as a kind of two-stroke engine. This chemical strategy manifests an unprecedented catalytic role for CoA N2″, substrate destabilization,[16,64] enzyme selection for near-attack configurations,[65] and the electrostatic preorganization of active sites,[66] each requiring precise protein conformational control. Transferase enzymes in general undergo larger conformational changes than hydrolases,[67] even when enzymes from the same superfamily are compared,[68] a finding that underscores the widely accepted role

of protein motions in regulating access to labile intermediates. The dynamic assembly of a competent tandem catalytic site may provide yet another tool for suppressing unproductive side reactions by class I CoA-transferases.

Furthermore, the conserved protein fold and constellation of active-site residues strongly imply a common mechanism for all class I CoA-transferases.

Comparison to Class III CoA-Transferases. The kinetic mechanisms for class I and class III CoA-transferases differ,[18,69,70] with the latter forming a pivotal aspartyl-CoA thioester complex that contains two carboxylates.[19] The results presented here show that there are differences all along the reaction coordinate. Structures of *Oxalobacter formigenes* FRC complexes containing CoA, either alone (PDB entry 1p5r) or with acylaspartyl anhydride adducts (PDB entries 1t4c and 2vjm), bind CoA in the same location, but the CoA moiety shifts substantially in the aspartyl-CoA thioester adduct (PDB entries 2vjk and 2vjm).[18,19,71] The motion propagates along the entire length of CoA, with some atoms moving 9 Å. In each anhydride adduct, CoA N2″ is at least 5 Å from either anhydride carbonyl oxygen and moves 5 Å in the conversion between anhydride and CoA adducts. These observations are incompatible with any catalytic role for CoA N2″ in class III CoA-transferase chemistry and are very different from those for the fixed CoA conformation observed here in comparable AarC adducts.

Relative to AarC, FRC appears to move very little during the reaction sequence, outside a mobile, glycine-rich loop that is proposed to protect labile enzyme intermediates[71] and binds oxalate at a substantial remove from the site of catalysis.[19,72] This region may perform a role similar to that of the AarC auxiliary site, Val270 gate, or both (see below). Even though they use the same sequence of reactions, class I and class III CoA-transferases employ different kinetic mechanisms. Moreover, these enzyme superfamilies appear to use fundamentally different chemical strategies that are not the result of convergent evolution.

Substrate Selection. Class I CoA-transferase enzyme chemistry is closely coordinated with a protein conformational cycle that has been likened to breathing.[73] Enzyme closure induced by acyl-CoA binding (Figure 4) creates an environment suitable for acyl transfer chemistry and protects labile intermediates (Figure 9B,C). Within the catalytic pocket, class I CoA-transferases have been proposed to recognize distal functional groups in preferred carboxylate or acyl-CoA substrates using chemically diverse side chains (e.g., Ser71) identified by model building.[12,13,74] Each set of residues is conserved only within a subset of functionally related class I CoA-transferases, consistent with roles in substrate selection. Good substrates allow complete enzyme closure (Figure 9) and the resulting immobilization of reactive groups.[7] Poor substrates that are too large [e.g., methylsuccinate (Table 1)] may interfere with the critical clamping, desolvation, and hydrogen bonding functions of Val270.

Carboxylate product formation (Figure 1) accompanies partial enzyme reopening, to allow carboxylate exchange (Figure 9D). Rapid carboxylate exchange may suppress unproductive hydrolysis of the glutamyl-CoA thioester adduct. Val270 defines one side of the aperture, which is wide enough to admit acetate and succinate to the catalytic pocket but not large carboxylates like citrate. Like Val227 in *Yersinia pestis* RipA,[74] Val270 appears to be a dynamic "gating" residue.[75−77] Therefore, Val270 has a dual influence on carboxylate substrate selectivity, as a gate and as a clamp.

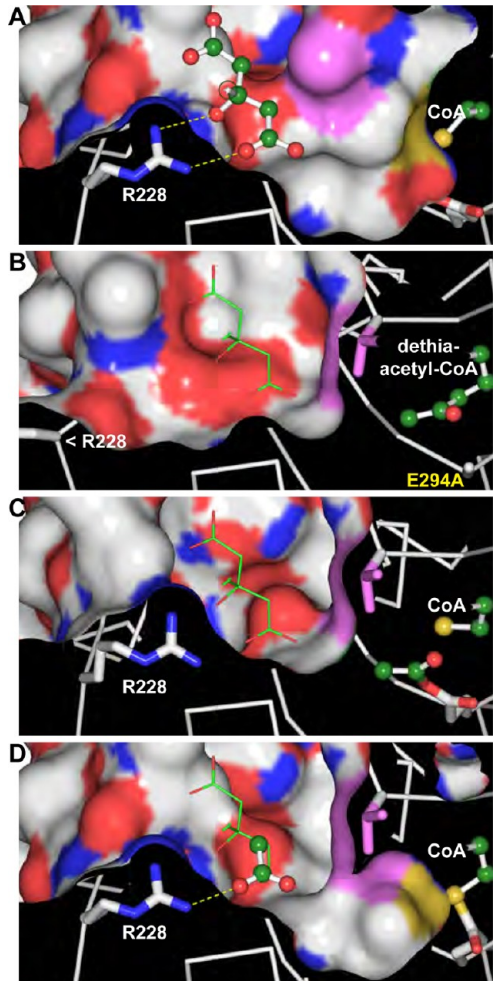

Figure 9. Regulation of carboxylate access to the active-site glutamate. Val270 forms part of a dynamic aperture separating the auxiliary carboxylate binding site from the catalytic pocket. The active-site cleft is shown in cross section, narrowing from the top left to the catalytic pocket adjacent to Glu294. The clipping plane for all panels is placed at the narrowest point (~3.5 Å) of the aperture. Ser71 is located at the bottom of each panel between the viewer and the clipping plane. Ligand atoms and backbone atoms are rendered in ball-and-stick and ribbon representations, respectively. Val270 C^{β} and C^{γ} are colored purple. The interior of the protein is colored black. Structures in panels B−D were aligned on the structure in panel A. Citrate from the complex in panel A is shown as thin green lines in other panels; in all panels, the central carboxylate is hidden by the clipping plane. (A) The AarCH6·CoA·citrate complex (PDB entry 4eu7, subunit B) adopts the open conformation. (B) The AarCH6-E294A·dethiaacetyl-CoA complex (PDB entry 4euc, subunit B) adopts the closed conformation with Arg228 extruded from the active site. The clipping plane was moved toward the viewer by 0.8 Å for the acetyl atoms only. Additional structures possessing Arg228 or Glu228 in the outward orientation are illustrated in Figure S14 of the Supporting Information. (C) The AarCH6·CoA·acetate complex (acetylglutamyl anhydride adduct, PDB entry 4eu6, subunit A) adopts the closed conformation. (D) The AarCH6·CoA·acetate complex (glutamyl-CoA thioester adduct, PDB entry 4eu6, subunit B) adopts the closed conformation. To the right of the aperture, the catalytic pocket is empty. High relative *B* factors for the loop containing Val270 suggest conformational motion that could have allowed acetate to leave the catalytic pocket.

dx.doi.org/10.1021/bi300957f | *Biochemistry* 2012, 51, 8422−8434

Class I CoA-transferases appear to use positive potential in the active-site cleft to recruit carboxylate substrates,[51,74] like several enzymes that catalyze diffusion-limited conversions of anionic substrates.[78−81] AarC has presumably been subject to strong selection for the efficient conversion of acetate to acetyl-CoA, consistent with a high k_{cat} value (Table S4 of the Supporting Information).[28] One such adaptation may be an auxiliary carboxylate site located outside the catalytic pocket near gating residue Val270, which contains the dynamic, AarC-specific residue Arg228 (Figure 9A). Studies of AarCH6-R228E indicate that Arg228 has an important kinetic role in carboxylate substrate binding. The auxiliary site nonselectively binds carboxylates at the threshold of the catalytic pocket, while selectivity is enforced by the conserved gating residue Val270 and the interior of the catalytic pocket. Binding of ≤2 mM acetate produced by acetyl-CoA cleavage (Figure 3D) suggests that the auxiliary site is traversed by carboxylates entering or exiting the catalytic pocket. Conformational changes that expel Arg228 from the vicinity of the active site may further increase the rate of carboxylate product dissociation.

SUMMARY

AarC evolved to play a primary metabolic role as SCACT under the selective pressure induced by high concentrations of membrane-permeant acetic acid, producing a CoA-transferase with relatively high substrate specificity and high turnover numbers. A novel oxyanion hole configuration involving CoA stabilizes one of two tetrahedral intermediates formed less than 3 Å apart. The proposal by Jencks that CoA binding energy is diverted into protein conformational changes that accelerate catalysis is fully substantiated by crystallographic depictions of what seems to be a common mechanism for class I CoA-transferases. An auxiliary binding site just outside the catalytic pocket appears to preconcentrate carboxylate substrates and might explain the relatively efficient conversion of the physiological substrate acetate.

ASSOCIATED CONTENT

Supporting Information

Methods for protein purification, CD analysis, ESI-TOF-MS analysis, and alignment of structures and sequences, oligodeoxynucleotide sequences (Table S1), isolation of AarC (Table S2), ESI-TOF-MS data (Table S3), kinetic data for alternate substrates (Table S4), substrate promiscuity data (Tables S5−S7), X-ray crystallographic data collection and refinement statistics (Tables S8−S11), atomic coordinates for modeled atoms (Tables S12−S16), conserved catalytic residues in diverse class I CoA-transferases (Table S17), class I CoA-transferase structural and functional data (Table S18), steady-state kinetic data for AarCH6 mutants (Table S19), acetate saturation curves (Figure S1), CD analysis (Figures S2−S4), citrate inhibition plot (Figure S5), crystal images (Figure S6), AarC topology diagram (Figure S7), chloride-site electron density maps (Figure S8), electrostatic surface renderings (Figure S9), CoA/citrate binding modes (Figure S10), acetylglutamyl anhydride adduct electron density maps (Figure S11), SCACT/4HBCT phylograms (Figure S12), structure-based sequence alignment (Figure S13), cutaway views of AarCH6 mutant active-site clefts (Figure S14), concentration-dependent AarCH6-S71A activity plot (Figure S15), conformational motions of AarCH6-S71A (Figures S16 and S17), and carboxylate saturation curves for AarCH6-R228E (Figure S18). This material is available free of charge via the Internet at http://pubs.acs.org.

AUTHOR INFORMATION

Corresponding Author

*E-mail: kappock@purdue.edu. Phone: (765) 494-8383. Fax: (765) 494-1897.

Funding

This work was supported by the Herman Frasch Foundation for Research in Agricultural Chemistry (531-HF02), the National Science Foundation (MCB 0936108 and MCB 0347250), and Purdue University Agricultural Research Programs. Use of the Advanced Photon Source was supported by the U.S. Department of Energy, Office of Science, Office of Basic Energy Sciences, under Contract DE-AC02-06CH11357. Use of LS-CAT Sector 21 was supported by the Michigan Economic Development Corp. and the Michigan Technology Tri-Corridor for the support of this research program (Grant 085P1000817).

Notes

The authors declare no competing financial interest.

ACKNOWLEDGMENTS

We thank Hong Jiang and Aaron Ransome for preparing dethiaacetyl-CoA, Kayleigh Nyffeler for help with mutant protein isolations, Kelly Sullivan for gel-filtration analysis, Spencer Anderson for collecting anomalous X-ray data, and Barb Golden for advice on refinement methods.

ABBREVIATIONS

4HBCT, 4-hydroxybutyrate CoA-transferase; AAB, acetic acid bacteria; aar, acetic acid resistance; AarC, SCACT from *A. aceti*; AarCH6, AarC with a C-terminal hexahistidine tag; CAC, citric acid cycle; CD, circular dichroism; CoA, coenzyme A; ESI-TOF-MS, electrospray ionization time-of-flight mass spectrometry; FRC, formyl-CoA transferase; NCS, noncrystallographic symmetry; ODN, oligodeoxynucleotide; PCT, propionate CoA-transferase; PDB, Protein Data Bank; rmsd, root-mean-square deviation; SCACT, succinyl-CoA:acetate CoA-transferase; SCOT, succinyl-CoA:3-oxoacid CoA-transferase; wt, wild-type.

ADDITIONAL NOTES

[a]The mismatched active sites may be the result of tight crystal packing in the vicinity of subunit A (primarily acetylglutamyl anhydride adduct), in which the CoA 3′-phosphate interacts with N^{ϵ} of Lys240B in an adjacent asymmetric unit. The active site in subunit B (primarily glutamyl-CoA thioester adduct) is more accessible. A similar phenomenon may have allowed the detection of an aspartyloxalyl anhydride adduct in one subunit of the class III CoA-transferase FRC.[18]

[b]In some distantly related class I CoA-transferases, Asn347 appears to be functionally replaced by Gln99 (SCOT numbering).

REFERENCES

(1) Jencks, W. P. (1973) In *The Enzymes* (Boyer, P. D., Ed.) Vol. 9, Chapter 11, pp 483−496, Academic Press, San Diego.

(2) Hersh, L. B., and Jencks, W. P. (1967) Coenzyme A transferase. Kinetics and exchange reactions. *J. Biol. Chem. 242,* 3468−3480.

(3) Hersh, L. B., and Jencks, W. P. (1967) Coenzyme A transferase. Isolation and properties of an enzyme-coenzyme A intermediate. *J. Biol. Chem. 242*, 3481−3486.
(4) Hersh, L. B., and Jencks, W. P. (1967) Isolation of an enzyme-coenzyme A intermediate from succinyl coenzyme A-acetoacetate coenzyme A transferase. *J. Biol. Chem. 242*, 339−340.
(5) Solomon, F., and Jencks, W. P. (1969) Identification of an enzyme-γ-glutamyl coenzyme A intermediate from coenzyme A transferase. *J. Biol. Chem. 244*, 1079−1081.
(6) Pickart, C. M., and Jencks, W. P. (1979) Formation of stable anhydrides from CoA transferase and hydroxamic acids. *J. Biol. Chem. 254*, 9120−9129.
(7) White, H., and Jencks, W. P. (1976) Mechanism and specificity of succinyl-CoA:3-ketoacid coenzyme A transferase. *J. Biol. Chem. 251*, 1688−1699.
(8) White, H., Solomon, F., and Jencks, W. P. (1976) Utilization of the inactivation rate of coenzyme A transferase by thiol reagents to determine properties of the enzyme-CoA intermediate. *J. Biol. Chem. 251*, 1700−1707.
(9) Moore, S. A., and Jencks, W. P. (1982) Formation of active site thiol esters of CoA transferase and the dependence of catalysis on specific binding interactions. *J. Biol. Chem. 257*, 10893−10907.
(10) Fierke, C. A., and Jencks, W. P. (1986) Two functional domains of coenzyme A activate catalysis by coenzyme A transferase. Pantetheine and adenosine 3′-phosphate 5′-diphosphate. *J. Biol. Chem. 261*, 7603−7606.
(11) Whitty, A., Fierke, C. A., and Jencks, W. P. (1995) Role of binding energy with coenzyme A in catalysis by 3-oxoacid coenzyme A transferase. *Biochemistry 34*, 11678−11689.
(12) Bateman, K. S., Brownie, E. R., Wolodko, W. T., and Fraser, M. E. (2002) Structure of the mammalian CoA transferase from pig heart. *Biochemistry 41*, 14455−14462.
(13) Tammam, S. D., Rochet, J.-C., and Fraser, M. E. (2007) Identification of the cysteine residue exposed by the conformational change in pig heart succinyl-CoA:3-ketoacid coenzyme A transferase on binding coenzyme A. *Biochemistry 46*, 10852−10863.
(14) Rangarajan, E. S., Li, Y., Ajamian, E., Iannuzzi, P., Kernaghan, S. D., Fraser, M. E., Cygler, M., and Matte, A. (2005) Crystallographic trapping of the glutamyl-CoA thioester intermediate of family I CoA transferases. *J. Biol. Chem. 280*, 42919−42928.
(15) Fraser, M. E., Hayakawa, K., and Brown, W. D. (2010) Catalytic role of the conformational change in succinyl-CoA:3-oxoacid CoA transferase on binding CoA. *Biochemistry 49*, 10319−10328.
(16) Jencks, W. P. (1987) Economics of enzyme catalysis. *Cold Spring Harbor Symp. Quant. Biol. 52*, 65−73.
(17) Heider, J. (2001) A new family of CoA-transferases. *FEBS Lett. 509*, 345−349.
(18) Jonsson, S., Ricagno, S., Lindqvist, Y., and Richards, N. G. J. (2004) Kinetic and mechanistic characterization of the formyl-CoA transferase from *Oxalobacter formigenes*. *J. Biol. Chem. 279*, 36003−36012.
(19) Berthold, C. L., Toyota, C. G., Richards, N. G. J., and Lindqvist, Y. (2008) Reinvestigation of the catalytic mechanism of formyl-CoA transferase, a class III CoA-transferase. *J. Biol. Chem. 283*, 6519−6529.
(20) Fukaya, M., Takemura, H., Okumura, H., Kawamura, Y., Horinouchi, S., and Beppu, T. (1990) Cloning of genes responsible for acetic acid resistance in *Acetobacter aceti*. *J. Bacteriol. 172*, 2096−2104.
(21) Fukaya, M., Takemura, H., Tayama, K., Okumura, H., Kawamura, Y., Horinouchi, S., and Beppu, T. (1993) The *aarC* gene responsible for acetic acid assimilation confers acetic acid resistance on *Acetobacter aceti*. *J. Ferment. Bioeng. 76*, 270−276.
(22) Ohmori, S., Masai, H., Arima, K., and Beppu, T. (1980) Isolation and identification of acetic acid bacteria for submerged acetic acid fermentation at high temperature. *Agric. Biol. Chem. 44*, 2901−2906.
(23) Ohmori, S., Uozumi, T., and Beppu, T. (1982) Loss of acetic acid resistance and ethanol oxidizing ability in an *Acetobacter* strain. *Agric. Biol. Chem. 46*, 381−389.
(24) Nakano, S., and Fukaya, M. (2008) Analysis of proteins responsive to acetic acid in *Acetobacter*: Molecular mechanisms conferring acetic acid resistance in acetic acid bacteria. *Int. J. Food Microbiol. 125*, 54−59.
(25) Francois, J. A., and Kappock, T. J. (2007) Alanine racemase from the acidophile *Acetobacter aceti*. *Protein Expression Purif. 51*, 39−48.
(26) Azuma, Y., Hosoyama, A., Matsutani, M., Furuya, N., Horikawa, H., Harada, T., Hirakawa, H., Kuhara, S., Matsushita, K., Fujita, N., and Shirai, M. (2009) Whole-genome analyses reveal genetic instability of *Acetobacter pasteurianus*. *Nucleic Acids Res. 37*, 5768−5783.
(27) Sakurai, K., Arai, H., Ishii, M., and Igarashi, Y. (2011) Transcriptome response to different carbon sources in *Acetobacter aceti*. *Microbiology 157*, 899−910.
(28) Mullins, E. A., Francois, J. A., and Kappock, T. J. (2008) A specialized citric acid cycle requiring succinyl-coenzyme A (CoA):acetate CoA-transferase (AarC) confers acetic acid resistance on the acidophile *Acetobacter aceti*. *J. Bacteriol. 190*, 4933−4940.
(29) Cole, P. A. (1996) Chaperone-assisted protein expression. *Structure 4*, 239−242.
(30) Francois, J. A., Starks, C. M., Sivanuntakorn, S., Jiang, H., Ransome, A. E., Nam, J.-W., Constantine, C. Z., and Kappock, T. J. (2006) Structure of a NADH-insensitive hexameric citrate synthase that resists acid inactivation. *Biochemistry 45*, 13487−13499.
(31) Bradford, M. M. (1976) A rapid and sensitive method for the quantitation of microgram quantities of protein utilizing the principle of protein-dye binding. *Anal. Biochem. 72*, 248−254.
(32) Nath, A., and Atkins, W. M. (2008) A quantitative index of substrate promiscuity. *Biochemistry 47*, 157−166.
(33) Teng, T.-Y. (1990) Mounting of crystals for macromolecular crystallography in a free-standing thin film. *J. Appl. Crystallogr. 23*, 387−391.
(34) Otwinowski, Z., and Minor, W. (1997) Processing of X-ray diffraction data collected in oscillation mode. *Methods Enzymol. 276*, 307−326.
(35) Guex, N., and Peitsch, M. C. (1997) SWISS-MODEL and the Swiss-PdbViewer: An environment for comparative protein modeling. *Electrophoresis 18*, 2714−2723.
(36) Adams, P. D., et al. (2010) *PHENIX*: A comprehensive Python-based system for macromolecular structure solution. *Acta Crystallogr. D66*, 213−221.
(37) Emsley, P., Lohkamp, B., Scott, W. G., and Cowtan, K. (2010) Features and development of *Coot*. *Acta Crystallogr. D66*, 486−501.
(38) Kleywegt, G. J. (2007) Crystallographic refinement of ligand complexes. *Acta Crystallogr. D63*, 94−100.
(39) DeLano, W. L. (2002) *The PyMOL molecular graphics system*, DeLano Scientific, Palo Alto, CA.
(40) Dolinsky, T. J., Nielsen, J. E., McCammon, J. A., and Baker, N. A. (2004) PDB2PQR: An automated pipeline for the setup of Poisson-Boltzmann electrostatics calculations. *Nucleic Acids Res. 32*, W665−W667.
(41) Baker, N. A., Sept, D., Joseph, S., Holst, M. J., and McCammon, J. A. (2001) Electrostatics of nanosystems: Application to microtubules and the ribosome. *Proc. Natl. Acad. Sci. U.S.A. 98*, 10037−10041.
(42) Miroux, B., and Walker, J. E. (1996) Over-production of proteins in *Escherichia coli*: Mutant hosts that allow synthesis of some membrane proteins and globular proteins at high levels. *J. Mol. Biol. 260*, 289−298.
(43) Francis, D. M., and Page, R. (2001) In *Current Protocols in Protein Science* (Coligan, J. E., Dunn, B. M., Ploegh, H. L., Speicher, D. W., and Wingfield, P. T., Eds.) Chapter 61, pp 5.24.1−5.24.29, Wiley, New York.
(44) Menzel, U., and Gottschalk, G. (1985) The internal pH of *Acetobacterium wieringae* and *Acetobacter aceti* during growth and production of acetic acid. *Arch. Microbiol. 143*, 47−51.
(45) Constantine, C. Z., Starks, C. M., Mill, C. P., Ransome, A. E., Karpowicz, S. J., Francois, J. A., Goodman, R. A., and Kappock, T. J. (2006) Biochemical and structural studies of N^5-carboxyaminoimida-

zole ribonucleotide mutase (PurE) from the acidophilic bacterium *Acetobacter aceti*. *Biochemistry 45*, 8193−8208.
(46) Mullins, E. A., Starks, C. M., Francois, J. A., Sael, L., Kihara, D., and Kappock, T. J. (2012) Formyl-coenzyme A (CoA):oxalate CoA-transferase from the acidophile *Acetobacter aceti* has a distinctive electrostatic surface and inherent acid stability. *Protein Sci. 21*, 686−696.
(47) Buckel, W., Dorn, U., and Semmler, R. (1981) Glutaconate CoA-transferase from *Acidaminococcus fermentans*. *Eur. J. Biochem. 118*, 315−321.
(48) Haller, T., Buckel, T., Rétey, J., and Gerlt, J. A. (2000) Discovering new enzymes and metabolic pathways: Conversion of succinate to propionate by *Escherichia coli*. *Biochemistry 39*, 4622−4629.
(49) Selmer, T., Willanzheimer, A., and Hetzel, M. (2002) Propionate CoA-transferase from *Clostridium propionicum*. Cloning of gene and identification of glutamate 324 at the active site. *Eur. J. Biochem. 269*, 372−380.
(50) Fleck, C. B., and Brock, M. (2008) Characterization of an acyl-CoA:carboxylate CoA-transferase from *Aspergillus nidulans* involved in propionyl-CoA detoxification. *Mol. Microbiol. 68*, 642−656.
(51) Jacob, U., Mack, M., Clausen, T., Huber, R., Buckel, W., and Messerschmidt, A. (1997) Glutaconate CoA-transferase from *Acidaminococcus fermentans*: The crystal structure reveals homology with other CoA-transferases. *Structure 5*, 415−426.
(52) Carson, M., Johnson, D. H., McDonald, H., Brouillette, C., and Delucas, L. J. (2007) His-tag impact on structure. *Acta Crystallogr. D63*, 295−301.
(53) Wu, W.-J., Anderson, V. E., Raleigh, D. P., and Tonge, P. J. (1997) Structure of hexadienoyl-CoA bound to enoyl-CoA hydratase determined by transferred nuclear Overhauser effect measurements: Mechanistic predictions based on the X-ray structure of 4-(chlorobenzoyl)-CoA dehalogenase. *Biochemistry 36*, 2211−2220.
(54) Martin, D. P., Bibart, R. T., and Drueckhammer, D. G. (1994) Synthesis of novel analogs of acetyl coenzyme A: Mimics of enzyme reaction intermediates. *J. Am. Chem. Soc. 116*, 4660−4668.
(55) Bürgi, H. B., Dunitz, J. D., and Shefter, E. (1973) Geometrical reaction coordinates. II. Nucleophilic addition to a carbonyl group. *J. Am. Chem. Soc. 95*, 5065−5067.
(56) Allen, S. H. G., Kellermeyer, R. W., Stjernholm, R. L., and Wood, H. G. (1964) Purification and properties of enzymes involved in the propionic acid fermentation. *J. Bacteriol. 87*, 171−187.
(57) Söhling, B., and Gottschalk, G. (1996) Molecular analysis of the anaerobic succinate degradation pathway in *Clostridium kluyveri*. *J. Bacteriol. 178*, 871−880.
(58) Scherf, U., and Buckel, W. (1991) Purification and properties of 4-hydroxybutyrate coenzyme A transferase from *Clostridium aminobutyricum*. *Appl. Environ. Microbiol. 57*, 2699−2702.
(59) Macieira, S., Zhang, J., Velarde, M., Buckel, W., and Messerschmidt, A. (2009) Crystal structure of 4-hydroxybutyrate CoA-transferase from *Clostridium aminobutyricum*. *Biol. Chem. 390*, 1251−1263.
(60) Mack, M., and Buckel, W. (1997) Conversion of glutaconate CoA-transferase from *Acidaminococcus fermentans* into an acyl-CoA hydrolase by site-directed mutagenesis. *FEBS Lett. 405*, 209−212.
(61) Hammes, G. G. (2002) Multiple conformational changes in enzyme catalysis. *Biochemistry 41*, 8221−8228.
(62) Koshland, D. E., Jr. (1960) The active site and enzyme action. *Adv. Enzymol. Relat. Subj. Biochem. 22*, 45−97.
(63) Gandour, R. D. (1981) On the importance of orientation in general base catalysis by carboxylate. *Bioorg. Chem. 10*, 169−176.
(64) Chan, K. K., Wood, B. M., Fedorov, A. A., Fedorov, E. V., Imker, H. J., Amyes, T. L., Richard, J. P., Almo, S. C., and Gerlt, J. A. (2009) Mechanism of the orotidine 5′-monophosphate decarboxylase-catalyzed reaction: Evidence for substrate destabilization. *Biochemistry 48*, 5518−5531.
(65) Bruice, T. C. (2002) A view at the millennium: The efficiency of enzymatic catalysis. *Acc. Chem. Res. 35*, 139−148.
(66) Kamerlin, S. C. L., Chu, Z. T., and Warshel, A. (2010) On catalytic preorganization in oxyanion holes: Highlighting the problems with the gas-phase modeling of oxyanion holes and illustrating the need for complete enzyme models. *J. Org. Chem. 75*, 6391−6401.
(67) Koike, R., Amemiya, T., Ota, M., and Kidera, A. (2008) Protein structural change upon ligand binding correlates with enzymatic reaction mechanism. *J. Mol. Biol. 379*, 397−401.
(68) Koike, R., Kidera, A., and Ota, M. (2009) Alteration of oligomeric state and domain architecture is essential for functional transformation between transferase and hydrolase with the same scaffold. *Protein Sci. 18*, 2060−2066.
(69) Dickert, S., Pierik, A. J., Linder, D., and Buckel, W. (2000) The involvement of coenzyme A esters in the dehydration of (*R*)-phenyllactate to (*E*)-cinnamate by *Clostridium sporogenes*. *Eur. J. Biochem. 267*, 3874−3884.
(70) Leutwein, C., and Heider, J. (2001) Succinyl-CoA:(*R*)-benzylsuccinate CoA-transferase: An enzyme of the anaerobic toluene catabolic pathway in denitrifying bacteria. *J. Bacteriol. 183*, 4288−4295.
(71) Ricagno, S., Jonsson, S., Richards, N., and Lindqvist, Y. (2003) Formyl-CoA transferase encloses the CoA binding site at the interface of an interlocked dimer. *EMBO J. 22*, 3210−3219.
(72) Gruez, A., Roig-Zamboni, V., Valencia, C., Campanacci, V., and Cambillau, C. (2003) The crystal structure of the *Escherichia coli* YfdW gene product reveals a new fold of two interlaced rings identifying a wide family of CoA transferases. *J. Biol. Chem. 278*, 34582−34586.
(73) Macieira, S., Zhang, J., Buckel, W., and Messerschmidt, A. (2012) Crystal structure of the complex between 4-hydroxybutyrate CoA-transferase from *Clostridium aminobutyricum* and CoA. *Arch. Microbiol. 194*, 157−166.
(74) Torres, R., Swift, R. V., Chim, N., Wheatley, N., Lan, B., Atwood, B. R., Pujol, C., Sankaran, B., Bliska, J. B., Amaro, R. E., and Goulding, C. W. (2011) Biochemical, structural and molecular dynamics analyses of the potential virulence factor RipA from *Yersinia pestis*. *PLoS One 6*, e25084.
(75) Zhou, H.-X., Wlodek, S. T., and McCammon, J. A. (1998) Conformation gating as a mechanism for enzyme specificity. *Proc. Natl. Acad. Sci. U.S.A. 95*, 9280−9283.
(76) Zhou, H.-X., and McCammon, J. A. (2010) The gates of ion channels and enzymes. *Trends Biochem. Sci. 35*, 179−185.
(77) McCammon, J. A. (2011) Gated diffusion-controlled reactions. *BMC Biophys. 4*, 4.
(78) Sheridan, R. P., and Allen, L. C. (1981) The active site electrostatic potential of human carbonic anhydrase. *J. Am. Chem. Soc. 103*, 1544−1550.
(79) Getzoff, E. D., Tainer, J. A., Weiner, P. K., Kollman, P. A., Richardson, J. S., and Richardson, D. C. (1983) Electrostatic recognition between superoxide and copper, zinc superoxide dismutase. *Nature 306*, 287−290.
(80) Ripoll, D. R., Faerman, C. H., Axelsen, P. H., Silman, I., and Sussman, J. L. (1993) An electrostatic mechanism for substrate guidance down the aromatic gorge of acetylcholinesterase. *Proc. Natl. Acad. Sci. U.S.A. 90*, 5128−5132.
(81) Tan, R. C., Truong, T. N., McCammon, J. A., and Sussman, J. L. (1993) Acetylcholinesterase: Electrostatic steering increases the rate of ligand binding. *Biochemistry 32*, 401−403.
(82) Korolev, S., Koroleva, O., Petterson, K., Gu, M., Collart, F., Dementieva, I., and Joachimiak, A. (2002) Autotracing of *Escherichia coli* acetate CoA-transferase α-subunit structure using 3.4 Å MAD and 1.9 Å native data. *Acta Crystallogr. D58*, 2116−2121.